applied sciences

MDPI

Article

Definition and Determination of Fin Substitution Factors Accelerating Thermal Simulations

Matthias Roppel *, Frank Rieg and Stephan Tremmel

Engineering Design and CAD, University of Bayreuth, Universitaetsstrasse 30, 95447 Bayreuth, Germany; frank.rieg@uni-bayreuth.de (F.R.); stephan.tremmel@uni-bayreuth.de (S.T.)

* Correspondence: matthias.roppel@uni-bayreuth.de

Abstract: The effort of numerical heat transfer calculations increases with the complexity and size of the domains and surfaces under consideration. When calculating heat transfers on finned arrays, one way to reduce this effort is to substitute the fins. Therefore, this work defines the fin substitution factor by considering that a smooth surface behaves thermally sufficiently similar to a specific finned array. A process for determining the case-specific most accurate analytical computation path for fin substitution factors is also defined. The performance of the process and the resulting solution is demonstrated using the example of vertical rectangular finned arrays under natural convective heat transfer with a constant fin base temperature and air as the surrounding fluid. The heat flows determined in solid-state simulations of flat plates considering fin substitution factors deviated by an average of 6.2% from the heat flows resulting from detailed CFD simulations of the corresponding finned arrays.

Keywords: thermal simulation; natural convection; CFD; FEM; fin substation factor

Citation: Roppel, M.; Rieg, F.; Tremmel, S. Definition and Determination of Fin Substitution Factors Accelerating Thermal Simulations. *Appl. Sci.* **2022**, *12*, 4449. https://doi.org/10.3390/app12094449

Academic Editors: Hernâni Miguel Reis Lopes and Elza Maria Morais Fonseca

Received: 31 March 2022
Accepted: 26 April 2022
Published: 28 April 2022

1. Introduction

The numerical simulation of natural convective heat transfer corresponds to the state of the art and is used in various cases. Especially when considering cooling fins, the focus is usually on analyzing the thermal processes or optimizing fin geometries and arrangements. Senapati et al. [1,2] examined the heat transfer to annular finned cylinders. His work focused on developing a Nusselt number correlation for the horizontal and vertical orientation and the investigation of the optimal fin spacing and fin-to-cylinder diameter ratio for these two cases. Wong et al. [3] carried out similar studies on horizontal annular finned cylinders, in which they also considered the influence of different fin materials. Mehrtash and Tari [4,5] investigated numerically flat plates with rectangular fins with different inclinations, whereby the fins were always oriented in the flow direction. Moreover, they defined correlations for estimating convective heat transfer rates. In contrast, Shen et al. [6] considered cross-flow rectangular finned arrays at different inclinations and presented a Nusselt number correlation for such cases.

In all the works mentioned above, numerical flow simulations were used. Depending on the fluid, its behavior, the geometry, and the level of detail, the computational effort can be very intensive. This is also because processes in the thermal and velocity boundary layer are decisive for the natural convective heat transfer [7]. To map the convective heat transfer with sufficient accuracy in numerical simulations, a sufficiently fine discretization of the flow domain and a suitable mapping of the near-wall turbulence are necessary. The larger and more complex the domain, the greater the calculation effort. Depending on the problem and the focus of the investigation, the computational effort can be reduced through various options, such as exploiting symmetry properties or using less computationally intensive material models and turbulence models [8].

When considering heat transfer processes on finned surfaces, there are more options to reduce the modeling and calculation effort. The simplest option is to assume a smooth

surface and neglect the fins, whereby conservative results are achieved [9]. Another option is to simulate smooth surfaces using experimentally determined, fin-specific factors. The purpose of such factors is that a smooth surface behaves thermally sufficiently similar to a specific finned array with its use. With such factors, it is possible to model, discretize and simulate only the geometrically simpler base body of the finned array [10,11]. However, the experimental determination of such factors is laborious, especially in the case of complex structures.

Such factors to simplify simulation models correspond to the state of the art and are available in various simulation programs. With Ansys Fluent, for example, it is possible to define a convective augmentation factor (CAF) or a specific roughness for a surface. With both, the heat transfer can be manipulated [10,12].

Regardless of the designation of the respective factors, the challenge is to calculate them correctly as long as there is no reliable experimental data. Following the authors' research, there is neither a clear definition nor a corresponding analytical calculation method for such factors yet. The present work contributes to closing this research gap by defining both the fin substitution factor (*FSF*) and a process for determining the best *FSF* analytical calculation method for certain boundary conditions. The approach is demonstrated in the example of vertical rectangular finned arrays considering natural convective heat transfer but can be applied to other fin profiles, fin orientations, and boundary conditions. With the approach presented in this work, thermal simulations of finned surfaces can be accelerated, both during modeling and during calculation.

2. Materials and Methods

In principle, the approach presented under Section 3 is suitable for different fin geometries and arrays as well as thermal and fluid dynamic boundary conditions. However, the approach is only demonstrated in a simplified special case.

Concerning the geometry of the fins and their orientation, only rectangular fins of a vertical finned array are considered because this is one of the best-studied cases.

For the same reason, air is chosen as the surrounding fluid.

The heat dissipation in finned arrays results from natural convection and thermal radiation. In the temperature range considered in this work, heat dissipation by natural convection dominates. However, it should be emphasized that the greater the temperature difference between the heat-emitting surface and the environment, the greater the proportion of heat that is dissipated by radiation [13]. In the following only natural convection is considered. There are two reasons for this: firstly, it is easier if the approach is only demonstrated using one heat transfer mechanism, and secondly, neglecting radiation leads to conservative results. However, thermal radiation can also be considered with the presented approach. This is possible, for example, by linearizing the thermal radiation and forming an effective heat transfer coefficient [13].

The space between two fins can be viewed as a semi-enclosed channel. Concerning the thermal boundary condition, when determining the Nusselt numbers in such channels, a distinction is made between a constant temperature and a constant heat flow at the fin base. Only isothermal cases were considered.

In summary, the heat transfer of vertical rectangular finned arrays via natural convection with air as surrounding fluid and a constant fin base temperature was chosen as the demonstration case.

The approach requires analytical equations and empiric correlations as well as flow simulations (CFD) and solid-state simulations (FEM). Already existing equations and correlations for the selected demonstration case were used. The simulation models were also designed for the demonstration case. These and the material properties of the used air are described below.

2.1. Temperature-Dependent Properties of Air

Table 1 shows the used material properties of air, which are used in the formulas, correlations, and simulation models. An average temperature is calculated between the ambient and the fin base temperature if necessary. The properties of air are determined for this average temperature via linear interpolation.

Table 1. Temperature-dependent material properties of air [13].

T (K)	ρ (kg/m^3)	ν (kg/m s)	k (W/m K)	c_p (J/kg K)	β (1/K)
273	1.276×10^{0}	1.722×10^{-5}	2.436×10^{-2}	1.006×10^{3}	3.674×10^{-3}
293	1.189×10^{0}	1.821×10^{-5}	2.587×10^{-2}	1.006×10^{3}	3.421×10^{-3}
373	9.333×10^{-1}	2.190×10^{-5}	3.162×10^{-2}	1.011×10^{3}	2.684×10^{-3}
473	7.359×10^{-1}	2.605×10^{-5}	3.823×10^{-2}	1.025×10^{3}	2.115×10^{-3}
573	6.075×10^{-1}	2.981×10^{-5}	4.442×10^{-2}	1.045×10^{3}	1.745×10^{-3}

2.2. Analytical Formulas

The authors would like to point out that there is no claim to completeness concerning these formulas.

2.2.1. Surfaces of the Smooth and Finned Surface

Figure 1 shows the designations of a flat plate and a vertical rectangular finned array. The area of smooth surface A_0, which corresponds to the area of the finned array, is calculated as

$$A_0 = W \cdot L \tag{1}$$

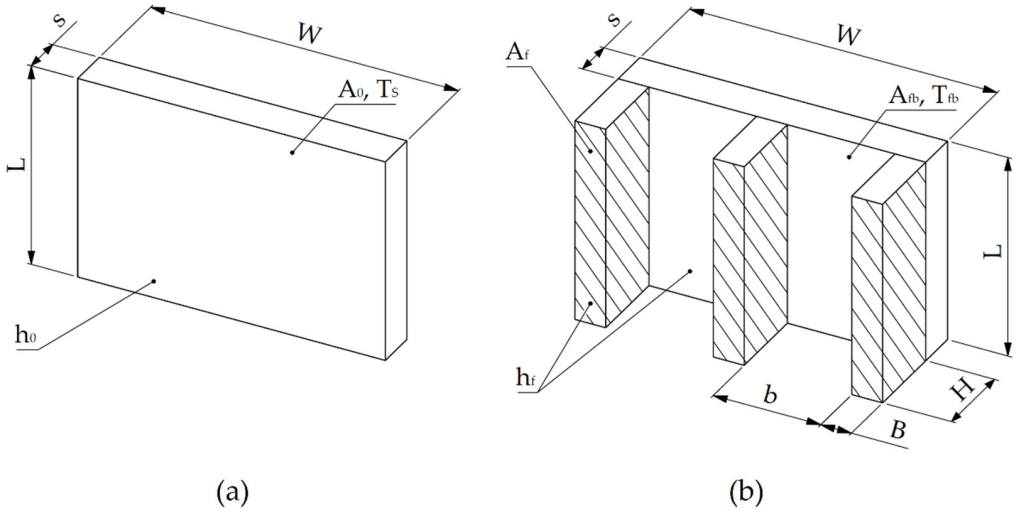

Figure 1. Schematic representation of a flat plate (**a**) and a vertical rectangular finned array (**b**).

Concerning the finned array, the perimeter P_f, the cross-sectional area $A_{f,cs}$, the surface area $A_{f,s}$, total fin area $A_{f,}$ and the fin base area A_{fb} are calculated using the formulas below. The end surfaces of the fin or the finned array are neglected.

$$P_f = 2H + B \tag{2}$$

$$A_{f,cs} = B\,L \tag{3}$$

$$A_{f,s} = (2H + B)\,L \tag{4}$$

$$A_f = A_{f,s}\,n \tag{5}$$

$$A_{fb} = b\,L\,n \tag{6}$$

2.2.2. Parameters for Plates

In general, heat transfer coefficients h can be calculated with the Nusselt number Nu, the thermal conductivity of the fluid k_{fluid}, and the characteristic length L_{spe} according to the following formula [14].

$$h = \frac{Nu\, k_{fluid}}{L_{spe}} \tag{7}$$

The case study shown in Section 3.3 requires the Nusselt numbers for vertical plates as well as for horizontal plates with both top and bottom heat dissipation. For the correlation of each Nusselt number, a specific Rayleigh number Ra has to be determined. This is calculated using the fluid-specific variables, density ρ, specific heat capacity c_p, thermal expansion coefficient β, kinematic viscosity ν, as well as the acceleration of gravity g and the temperature difference between the surface $T_{S,i}$ and the environment using the following formula [13].

$$Ra_i = \frac{c_{p,i}\, g\, \beta_i\, \rho_i\, (T_{S,i} - T_\infty)\, L_{spe,i}^3}{\upsilon_t\, k_{fluid,i}} \tag{8}$$

Every part of the Formula (8) is case-specific. One of these is the characteristic length, which describes the dimension that is decisive for convective heat transfer. With a vertical plate, the characteristic length corresponds to the height of the plate [13].

$$L_{spe,vp} = L \tag{9}$$

In the case of a horizontal plate with an upward or downward heat flow, it is calculated according to the following formula [13].

$$L_{spe,hp} = \frac{L\, W}{2\,(L + W)} \tag{10}$$

According to Churchill and Chu [15], Nusselt numbers for a vertical plate are determined using

$$Nu_{vp} = \left(0.825 + 0.387 \left(Ra_{vp} \left(1 + \left(\frac{0.492}{Pr}\right)^{\frac{9}{16}}\right)^{-\frac{16}{9}}\right)^{\frac{1}{6}}\right)^2 \tag{11}$$
$$\text{for } 10^{-1} < Ra_{vp} < 10^{12} \text{ and } 0.001 < Pr < \infty$$

A distinction must be made between laminar and turbulent flow for the Nusselt number of a horizontal plate with upward heat flow [16].

$$Nu_{hp,u\ lam} = 0.766 \left(Ra_{hp} \left(1 - \left(\frac{0.322}{Pr}\right)^{\frac{11}{20}}\right)^{-\frac{20}{11}}\right)^{\frac{1}{5}} \tag{12}$$
$$\text{for } 7 \times 10^4 < Ra_{hp}$$

$$Nu_{hp,u\ tur} = 0.15 \left(Ra_{hp} \left(1 - \left(\frac{0.322}{Pr}\right)^{\frac{11}{20}}\right)^{-\frac{20}{11}}\right)^{\frac{1}{3}} \tag{13}$$
$$\text{for } 7 \times 10^4 < Ra_{hp}$$

Only a laminar boundary layer flow is expected for a horizontal plate with a downward directed heat flow, even with large Rayleigh numbers. So the Nusselt number is calculated using the following formula [16].

$$Nu_{hp,u\ lam} = 0.766\left(Ra_{hp}\left(1-\left(\frac{0.322}{Pr}\right)^{\frac{11}{20}}\right)^{-\frac{20}{11}}\right)^{\frac{1}{5}} \quad \text{for } 7\times10^4 < Ra_{hp} \tag{14}$$

2.2.3. Parameters for Vertical Rectangular Finned Arrays

In contrast to flat plates, many Nusselt number correlations exist for vertical rectangular finned arrays. Regardless of the correlation, the characteristic length applies to vertical finned arrays [14]:

$$L_{spe,vfa} = L \tag{15}$$

Vertical channel flows can approximate flow and heat dissipation within vertical rectangular finned arrays. With such channels, the Rayleigh number has to be determined using the special formulation below, where thermal diffusivity α is used [17].

$$Ra_{vfa,T} = \frac{g\,\beta\,(T_s - T_\infty)\,b^3}{v\,\alpha}\,\frac{b}{L} \tag{16}$$

There are different Nusselt number correlations for vertical rectangular finned arrays based on experiments. In the course of this work, it will be worked out which of these correlations can be used to determine the *FSF* so that there is the highest possible thermal similarity between a smooth and a specific finned surface. Below, the correlations for isothermal boundary conditions are listed. The respective index refers to the author.

Elenbaas [18]:

$$Nu_{El} = \frac{Ra_{vfa,T}}{24}\left(1-e^{-\frac{35}{Ra_{vfa,T}}}\right)^{0.75} \tag{17}$$

Aihara [19]:

$$Nu_{Ai} = \frac{Ra_{vfa,T}}{24}\left(1-e^{-\frac{32.7}{Ra_{vfa,T}}}\right)^{0.75} \tag{18}$$

Bar-Cohen et al. [20]:

$$Nu_{Ba} = \left(\frac{576}{{Ra_{vfa,T}}^2} + \frac{2.873}{\sqrt{Ra_{vfa,T}}}\right)^{-0.5} \tag{19}$$

Rohsenow et al. [21]:

$$Nu_{Ro} = \left(\left(\frac{Ra_{vfa,T}}{24}\right)^{-1.9} + \left(c_{Ro}C_{Ro}{Ra_{vfa,T}}^{0.25}\right)^{-1.9}\right)^{-\frac{1}{1.9}} \tag{20}$$

Olsson [22]:

$$Nu_{Ol} = \left(\left(\frac{Ra_{vfa,T}}{24}\right)^{-1.3} + \left(c_{Ro}C_{Ro}{Ra_{vfa,T}}^{0.25}\right)^{-1.3}\right)^{-\frac{1}{1.3}} \tag{21}$$

Concerning Formulas (20) and (21) c_{Ro} can take values between 1 and 1.32, and C_{Ro} has to be calculated according to the following equation [21].

$$C_{Ro} = \frac{0.671}{\left[1+\left(\frac{0.492}{Pr}\right)^{\frac{9}{16}}\right]^{\frac{4}{9}}} \tag{22}$$

An ideal fin would have an infinitely high thermal conductivity, and therefore, the temperature at every point of the fin would be the same as at the fin base. As a result, a maximum heat flow could be given off to the environment. The fin efficiency η sets the transferable heat of a real fin Q_{real} in ratio to that one of an ideal fin Q_{ideal}. It is defined as [13]:

$$\eta_f = \frac{Q_{real}}{Q_{ideal}} = \frac{Q_{real}}{h_f \, A_{f,s} \left(T_{fb} - T_\infty \right)} \leq 1 \tag{23}$$

In addition to the heat transfer from solid to fluid, the heat transport in the fins must also be considered. This is possible via fin efficiency. It depends on the temperature distribution in the fin and the fin geometry. For rectangular fins with heat transfer via all fin surfaces, fin efficiency can be determined using the Biot Number Bi and in parameter μ [16].

$$\eta_f = \frac{1}{\mu \left(L + \frac{A_{f,cs}}{P_f} \right)} \frac{sinh(\mu L) + \frac{Bi}{\mu L} \, cosh(\mu L)}{cosh(\mu L) + + \frac{Bi}{\mu L} \, sinh(\mu L)} \tag{24}$$

$$\mu = \sqrt{\frac{h_f \, P_f}{k_f \, A_{f,cs}}} \tag{25}$$

$$Bi = \frac{h \, L_{spe}}{k_{fluid}} \tag{26}$$

2.3. Hardware and Software

In the course of this work, CFD and solid-state simulations were used. All simulations were performed with the academic version of ANSYS Workbench 2020 R2. ANSYS Fluent was used for the CFD simulations and the ANSYS Mechanical module steady-state thermal for the solid-state simulations. All simulations were performed on a Windows 10 64-bit PC with 18 Intel(R) Core(TM) i9-10980XE CPU @ 3.00 GHz (36 threads), 128 GB random access memory and 2 × 4 TB HDD data storage.

2.4. CFD Simulation Modeling

Only steady-state cases were considered. The dimensions of the fluid domain depend on the dimensions of the finned array, as shown in Figure 2a. Concerning the simplifications and the types of boundary conditions, the authors followed the modeling strategies of Senapati et al. [1] and Wong et al. [3]. Surfaces 1, 2, 3, 5, and 6 of the fluid domain had the boundary condition pressure outlet, with a backflow total temperature corresponding to the ambient temperature. Surface 4 was defined as an adiabatic wall. The constant fin base temperature was specified on the back of the fin base plate.

To model the heat transfer close to the wall with sufficient accuracy, the turbulence model and meshing had to be coordinated. Based on the results of Wu et al. [23] and Jeong et al. [24] the k-ω SST turbulence model was used. The computational domains were partitioned to create structured grids, see Figure 2b. In principle, the grid depends on the dimensions of the finned array under consideration. The meshing was controlled edge-specifically via the number of elements. The elements grew towards the flow domain starting from the fin surface, see Figure 2c. Depending on the case under consideration, the growth rate was between 5 and 8. For all used discretization, it was checked that the dimensionless wall distance y^+ at the solid-fluid interface was near 1 [12].

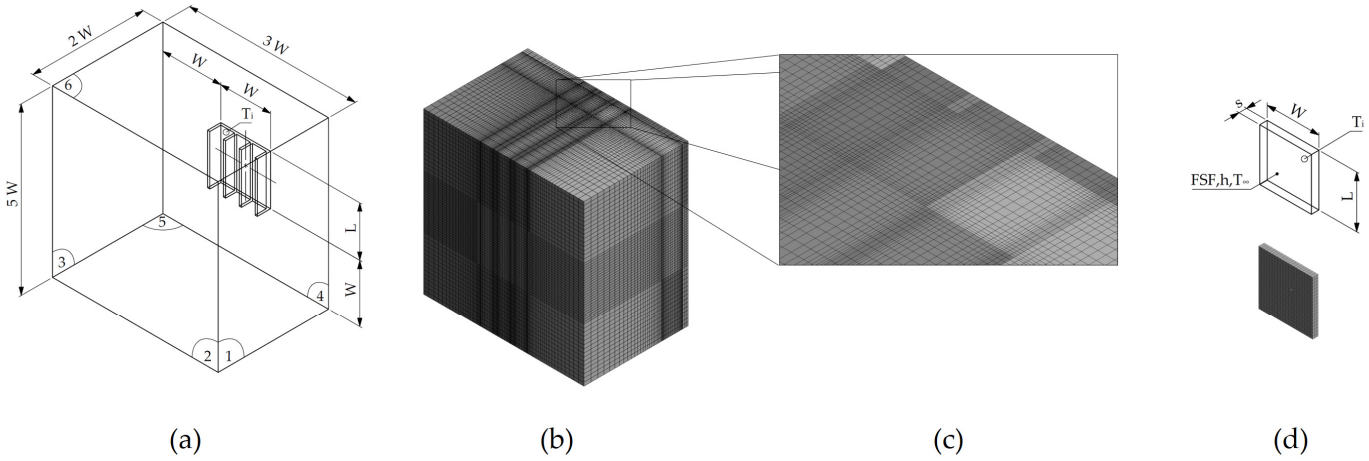

Figure 2. CFD simulation model (**a**), discretized CFD computational domain (**b**), a detailed CFD grid view (**c**), solid-state simulation model, and the meshed domain (**d**).

The fluid behavior was approximated by Boussinesq approximation and specified by the thermal expansion coefficient and the air density in each case at ambient temperature. Based on all simulations, a maximum fin base temperature of 473 K and a minimum ambient temperature of 293 K with a corresponding thermal expansion coefficient of 0.003421 1/K occurred. These values satisfy the following condition for using the Boussinesq approximation [12].

$$\beta \left(T_{fb} - T_{\infty} \right) = 0.616 \ll 1 \tag{27}$$

The maximum number of iterations was 500 for each simulation. Further simulation settings are summarized in Table 2.

Table 2. CFD simulation settings.

Parameter	Setting	Parameter	Setting
Solution Method		Residuals	
Pressure-Velocity-Coupling	Coupled	continuity	10^{-6}
Spatial Discretization		x-velocity	10^{-6}
Gradient	Least Square Cell Based	y-velocity	10^{-6}
Pressure	PRESTO!	z-velocity	10^{-6}
Momentum	Second Order Upwind	energy	10^{-6}
Turbulent Kinetic Energy	Second Order Upwind	k	10^{-6}
Specific Dissipation Rate	Second Order Upwind	ω	10^{-6}
Energy	Second Order Upwind		
Pseudo Transient			

2.5. Solid-State Simulation Modeling

The Finite-Element-Method (FEM) was used for solid-state simulations. Only steady-state cases were considered. Concerning the FEM simulation model, only the base plate of the respective finned array was considered, see Figure 2d. The corresponding temperature at the fin base was a boundary condition on a front surface. There was a convection boundary condition defined on the opposite front surface, with the ambient temperature and a variable heat transfer coefficient. Depending on the investigation, the case-specific product of a *FSF* and a heat transfer coefficient of a smooth surface were defined as the value for this variable heat transfer coefficient. The lateral surfaces of the plate also had convection boundary conditions. The corresponding parameters had to be calculated according to the formulas (Section 2.2.3). The structured mesh consisted of quadratic hexahedrons with an element size of 5 mm. A convergence study verified the mesh quality.

3. Results

3.1. Definition of the Fin Substitution Factor

A smooth surface should behave thermally sufficiently similar to a specific finned surface using the *FSF*. Thereby the smooth surface should have the same dimensions as the base plate of the finned array. Both surfaces are thermally similar if:

- Identical temperatures exist for the smooth surface and the fin base
- Identical heat flows of the smooth and the ripped surfaces

The *FSF* results from the heat flows of the smooth and the finned surfaces, shown in Figure 1, whereby the focus in this work is just on natural convective heat transfer. The convective heat flow Q_0 of a smooth surface is calculated by

$$Q_0 = h_0 \cdot A_0 \cdot (T_s - T_\infty) \tag{28}$$

and depends on the difference between the surface T_S and the ambient temperature T_∞, the size of the surface itself A_0, and the heat transfer coefficient h_0 [13,14]. The heat conduction in the fins must also be taken into account with a finned surface. This can be done via the thermal fin efficiency η. The heat flow of a finned surface Q_f can be determined using the heat transfer coefficient h_f, the areas of the fins A_f and the fin base A_{fb} and the temperature difference between the fin base T_{fb} and the ambient [13,14].

$$Q_f = h_f \cdot \left(A_{fb} + \eta \cdot A_f\right) \cdot \left(T_{fb} - T_\infty\right) \tag{29}$$

The *FSF* is defined as the ratio of the heat flow from the finned surface to the heat flow emitted by the smooth surface.

$$FSF = \frac{Q_f}{Q_O} = \frac{h_f \cdot \left(A_{fb} + \eta \cdot A_f\right) \cdot \left(T_{fb} - T_\infty\right)}{h_0 \cdot A_0 \cdot (T_s - T_\infty)} \tag{30}$$

Taking into account the objective that the temperature of the smooth surface should correspond to that one at the fin base, the definition of the *FSF* can be simplified as follows

$$FSF = \frac{Q_f}{Q_O} = \frac{h_f}{h_0} \cdot \frac{\left(A_{fb} + \eta \cdot A_f\right)}{A_0} \tag{31}$$

On closer examination of this definition, the *FSF* consists of parameters describing geometry (A_{fb}, A_f, A_0), heat conduction (η), and heat transfer (h_f, h_0).

3.2. Method for Determining Fin Substitution Factor

The challenge in determining the *FSF* is to define a suitable calculation path for a specific case. Therefore, a process is presented, which is shown schematically in Figure 3.

The task is to define an analytical *FSF* calculation path for a specific fin geometry and for specific thermal boundary conditions. The measure of the quality of the calculated *FSF* is its ability to produce the greatest possible thermal similarity between a smooth surface and the corresponding fin array.

In the first process step, many parameters must be specified. Thereby a distinction is necessary between high-level parameters and low-level parameters. The analytical formulas or empirical correlations used later in the process are decisive for this classification. Because some of these formulas only have a limited scope of application and validity. All parameters that are decisive for these restrictions are high-level parameters. These are:

- Shape of the fins
- Orientation of the finned array
- Type of surrounding fluid
- Type of the thermal boundary conditions

All other parameters of the analytical or analytical-empirical equations are low-level parameters. These parameters have to be varied to find the best *FSF* calculation path. These include:

- Geometric dimensions of the finned array
- Fluid and Material parameters
- Values of the thermal boundary conditions

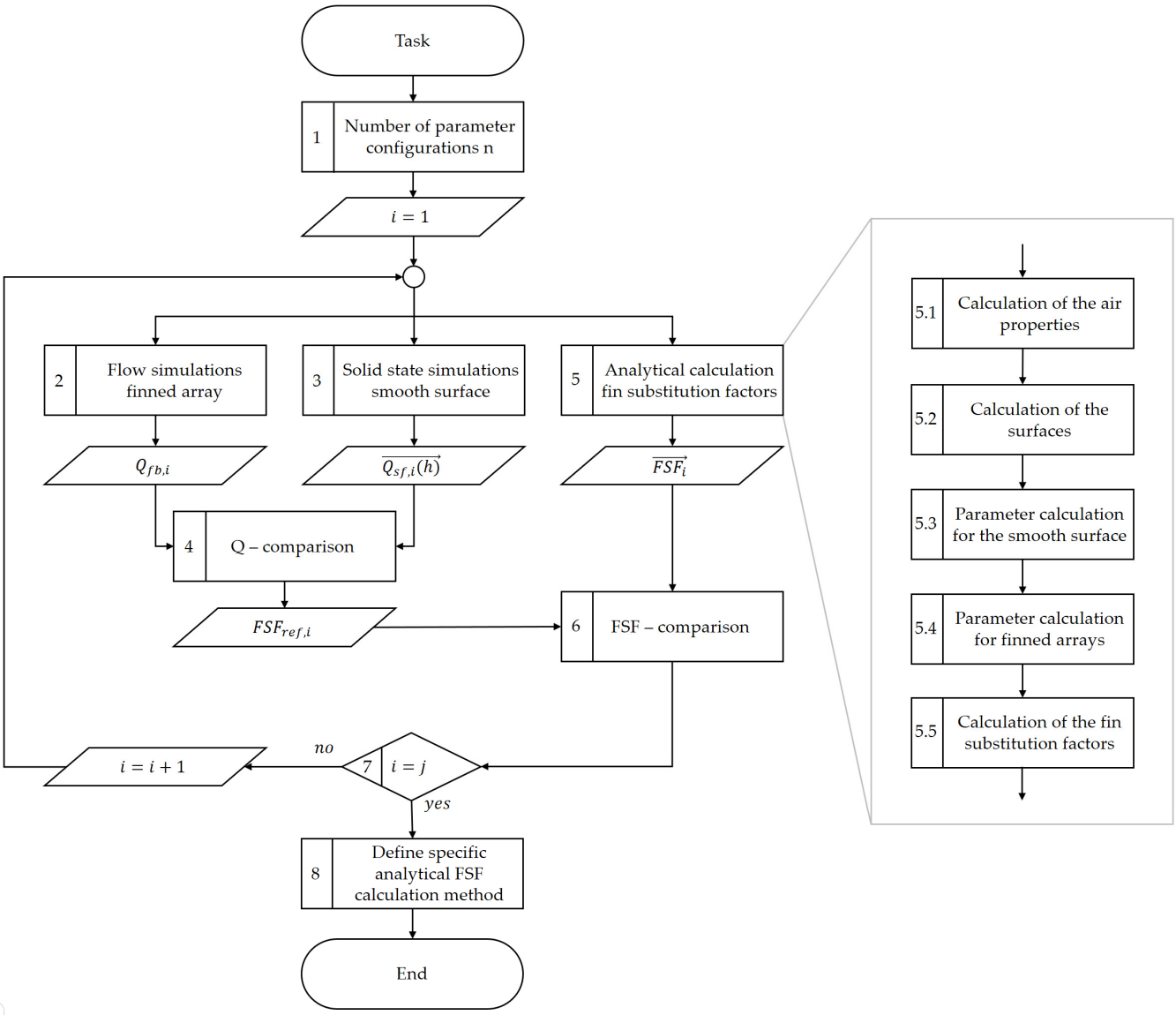

Figure 3. Process for determining the specific analytical *FSF* calculation method.

After defining the high-level parameters, any number j of configurations can be generated by varying the low-level parameters. The further process has to be run through once for each of these configurations. Basically, the larger the interval and the number of values of each low-level parameter, the more configurations can be considered, and the more general is the resulting analytical *FSF* calculation path of this process. Starting with the first configuration, $i = 1$, the following process steps have to be completed:

The second process step calculates the respective configuration in a detailed CFD simulation. It is important to ensure that the fluid domain around the finned array is large enough not to affect the heat transfer process. The discretization must be fine enough not to affect the result. The output of this step is a particular heat flow $Q_{fb,i}$, which is given off by the finned array under the given boundary conditions.

The third process step aims to determine a vector of manipulated heat flows from the smooth surface to the ambient air. Therefore, a large number of solid-state simulations are carried out. Only the smooth surface and the corresponding thermal boundary conditions at the fin base are considered within those simulations. The side where the fins are located obtains a convection boundary condition. The heat transfer coefficient of this boundary condition has to be varied in a certain interval. Investigations of the interval limits for this parameter for different cases have shown that it is sufficient to vary the heat transfer coefficient between 1 and 500 times that value, which can be determined analytically for the corresponding smooth surface. The output of this step is a vector of manipulated heat flows, depending on the heat transfer coefficient.

In the fourth process step, the heat flow of the second step is compared with each entry in the vector of the third step. This step aims to find out at which heat transfer coefficient the heat flow of the smooth surface (step 3) corresponds to that of one of the finned arrays (step 2). Interpolation is possible within certain limits. If a corresponding transfer coefficient is found, this ratio to the analytically determined one of the smooth surfaces has to be formed. This ratio is denoted as $FSF_{ref,i}$ and corresponds to the reference value to which the analytically determined FSF of the finned arrays (step 5) should deviate as little as possible.

The fifth process step aims to serve a vector of FSFs, where each entry results from a different analytical calculation path. In general, there are many equations and correlations to determine the various parameters of the chosen finned array. The difficulty is to find the combination of all these equations that will most accurately determine the FSF. For this purpose, all possible combinations of equations and correlations must be investigated, and the corresponding calculation path-dependent FSF must be formed. The output of this step is the vector of calculation path-dependent FSF_i. This vector is determined according to the subprocess also shown in Figure 3 with the following steps:

- Determination of the case-specific, temperature-dependent air properties
- Calculation of the surfaces of the smooth base body and the finned array
- Calculation of the parameters of the smooth surface
- Calculation of the finned array parameters
- Determination of the FSF_i vector

In the sixth process step, the FSF_{ref} (step 4) is compared with each entry in the vector of the fifth step. The evaluation can be done in different ways. In this work, the absolute deviation and the relative deviation according to the amount for each value FSF_i are calculated. The deviation can be calculated overall as well as low-level parameter-specifically. The end of this process step is a listing of calculation path-specific deviations.

The seventh process step has to be checked if the process has already been carried out for all configurations j. If this is not the case, the process must be repeated with the next configuration. Once all configurations have been considered, the deviations of all j step 6 have to be evaluated.

The evaluation is the eighth and final step of the process. The aim is to find out the calculation path whose FSF_i has the smallest deviations from the different FSF_{ref}. It may be necessary to make low-level parameter-specific definitions of the calculation path.

3.3. Case Study: Natural Convection on Vertical Rectangular Finned Arrays

3.3.1. Specifications

First of all, the high-level parameters had to be defined. For the demonstration case, these are:

- Shape of the fins: rectangular
- Orientation of the finned array: vertical
- Type of surrounding fluid: air
- Type of the thermal boundary conditions: constant temperature

Next, many low-level parameter combinations had to be investigated so that the analytical calculation path was also valid for a large area of application. Table 3 summarizes all low-level parameters that were varied in this work.

Table 3. Low-level parameters for calculation path determination.

Low-Level Parameters	Unit	Value
W	mm	180
s	mm	5
B	mm	3
k_{fin}	W/m K	130
T_{amb}	K	293
H	mm	12.5/25/50/100
L	mm	125/250/500
b	mm	8.8/14.7/32.4/56
n	-	4/6/11/16
T_{fb}	K	303/323/373/423/473

3.3.2. Objectives

Taking a closer look at Formula (31), the *FSF* consists of three components: geometry ratios (indicated by index A), heat conduction within the fin (indicated by index η), and the ratio of the heat transfer (indicated by index h). Especially the computational effort for the heat transfer coefficients is high. Therefore, the question is answered whether it is necessary to consider all components or whether a simplified calculation is sufficient. The following definitions of the *FSF* are used, whereby the indices indicate the considered components.

FSF depending on geometric quantities:

$$FSF_A = \frac{\left(A_{fb} + A_f\right)}{A_0} \tag{32}$$

FSF depending on geometric quantities and heat conduction in the fins:

$$FSF_{A,\eta} = \frac{\left(A_{fb} + \eta_f \cdot A_f\right)}{A_0} \tag{33}$$

FSF depending on geometric quantities and heat transfer:

$$FSF_{A,h} = \frac{h_f}{h_0} \cdot \frac{\left(A_{fb} + A_f\right)}{A_0} \tag{34}$$

FSF depending on geometric quantities, heat conduction, and heat transfer:

$$FSF_{A,\eta,h} = \frac{h_f}{h_0} \cdot \frac{\left(A_{fb} + \eta_f \cdot A_f\right)}{A_0} \tag{35}$$

In addition to the components, it is examined which Nusselt number correlation presented under Section 2.2.3 provides the best results for the considered parameter combinations, listed in Table 3.

3.3.3. Determination of the Calculation Path for Vertical Rectangular Finned Arrays

Due to this choice of parameters, the process shown in Figure 3 was carried out 240 times. A total of 240 flow simulations and 295 solid-state simulations were carried out.

For each low-level parameter combination, there was one $FSF_{ref,i}$ (output step 4), and a vector of analytically determined FSF_i (output step 5). In the course of each process step

6, the absolute and relative deviation according to the amount concerning the respective $FSF_{ref,i}$ was determined for each FSF_i. The deviations are determined using the heat flows. The heat flow, which resulted from the solid-state simulation in connection with the *FSF* of the respective calculation path, is always related to that heat flow, which was determined by the corresponding CFD simulation.

Process step 8 is for evaluation. For these two parameters the relative deviations according to the amount, Table 4, and the standard deviations formed from the absolute deviations, Table 5 are used. The indices of the *FSF* indicate the considered components (Formulas (32)–(35)) and the respective Nusselt number correlation (Formulas (17)–(21)). If a number is contained in the index, this refers to the used value of c_{Ro}. The deviations are specified in both overall and low-level parameters. The five *FSF* calculation paths with the most accurate results are highlighted for each low-level parameter.

Table 4. The relative deviation according to the amount of the heat flows results from the different *FSF*s concerning the respective reference heat flows $FSF_{ref,i}$. The smallest deviations are highlighted.

FSF	Overall	T_{fb} (K)					*H* (mm)				*L* (mm)			*b* (mm)			
		303	323	373	423	473	12.5	25	50	100	125	250	500	8.8	14.7	32.4	56.0
FSF_A	14.12	21.62	17.74	12.97	9.83	8.45	17.28	13.89	11.97	13.35	8.17	12.52	21.68	23.43	14.06	9.63	9.37
$FSF_{A,\eta,EL}$	12.86	17.93	12.57	9.41	10.55	13.84	15.78	11.97	11.77	11.91	10.65	11.47	16.45	19.80	11.98	9.53	10.12
$FSF_{A,\eta,Ai}$	12.67	17.95	12.59	9.25	10.20	13.37	15.84	12.01	11.61	11.24	10.44	11.27	16.30	19.75	11.83	9.24	9.88
$FSF_{A,\eta,Ba}$	12.82	17.92	12.55	9.36	10.49	13.78	15.78	11.96	11.73	11.81	10.61	11.43	16.42	19.85	11.94	9.44	10.04
$FSF_{A,\eta,Ro1}$	12.35	18.00	12.64	9.00	9.59	12.55	15.94	12.08	11.32	10.07	10.06	10.96	16.04	19.75	11.55	8.68	9.42
$FSF_{A,\eta,Ro1\cdot32}$	13.42	17.89	12.63	9.94	11.51	15.12	15.61	11.87	12.30	13.90	11.24	12.02	17.00	20.02	12.54	10.32	10.79
$FSF_{A,\eta,Ol1}$	13.42	17.99	12.72	9.98	11.44	14.96	15.64	11.91	12.32	13.82	11.22	12.00	17.05	20.12	12.69	10.26	10.61
$FSF_{A,\eta,Ol1\cdot32}$	14.94	18.13	13.14	11.51	13.83	18.08	15.29	11.87	14.02	18.56	12.70	13.58	18.53	20.48	14.37	12.42	12.48
$FSF_{A,h,EL}$	9.64	15.62	13.99	8.41	4.62	5.57	12.85	9.20	7.49	9.01	9.92	9.66	9.33	8.75	11.51	10.16	8.14
$FSF_{A,h,Ai}$	8.04	12.15	9.88	4.64	4.94	8.59	10.40	8.29	7.50	5.97	8.00	7.74	8.39	7.82	8.74	8.75	6.84
$FSF_{A,h,Ba}$	9.51	15.51	13.44	7.98	4.57	6.06	12.80	9.19	7.47	8.59	9.74	9.34	9.46	9.16	11.62	9.70	7.56
$FSF_{A,h,Ro1}$	9.65	6.53	4.09	6.95	12.18	18.50	9.80	10.49	12.12	6.19	9.34	8.58	11.02	9.25	8.42	10.41	10.52
$FSF_{A,h,Ro1\cdot32}$	17.92	23.84	23.33	18.99	14.01	9.44	21.87	17.02	13.97	18.83	18.87	18.53	16.37	14.68	21.94	18.22	16.86
$FSF_{A,h,Ol1}$	16.73	22.89	21.52	17.45	12.76	9.00	20.39	15.71	13.20	17.60	17.68	16.91	15.59	11.92	22.67	17.75	14.56
$FSF_{A,h,Ol1\cdot32}$	33.61	35.83	37.27	35.34	31.71	27.87	36.95	32.92	30.29	34.27	35.91	34.13	30.77	22.28	39.48	37.53	35.14
$FSF_{A,\eta,h,EL}$	11.58	11.91	9.42	8.49	11.46	16.62	11.52	9.20	11.62	13.97	8.70	10.26	15.79	12.79	12.08	11.50	9.95
$FSF_{A,\eta,h,Ai}$	12.71	9.42	7.98	9.69	15.12	21.37	9.89	9.73	14.03	17.21	9.01	11.24	17.89	13.81	12.62	12.75	11.68
$FSF_{A,\eta,h,Ba}$	11.83	12.06	9.29	8.57	11.97	17.25	11.54	9.31	12.04	14.43	8.84	10.33	16.32	12.89	12.30	11.77	10.36
$FSF_{A,\eta,h,Ro1}$	18.25	9.21	9.44	16.56	24.17	31.87	10.41	14.04	22.63	25.92	13.95	16.47	24.32	18.02	16.76	19.12	19.11
$FSF_{A,\eta,h,Ro1\cdot32}$	13.53	19.45	16.72	11.95	9.78	9.75	19.73	13.18	10.08	11.13	13.75	12.39	14.45	13.23	15.56	13.44	11.90
$FSF_{A,\eta,h,Ol1}$	13.47	19.14	15.88	11.60	10.00	10.74	18.34	12.81	10.72	12.01	12.88	12.05	15.48	13.78	15.85	13.27	10.98
$FSF_{A,\eta,h,Ol1\cdot32}$	25.78	31.66	30.62	26.30	21.80	18.51	34.80	28.26	21.44	18.62	30.41	25.55	21.38	18.26	29.64	28.37	26.83

3.3.4. Validation

In this item, the performance of the specified calculation path is demonstrated by using examples from the literature. Three rectangular finned arrays from different sources were considered with three constant fin base temperatures. For each of these nine cases, a CFD simulation was carried out. Because of the results of Section 3.3.3 for each case, the respective $FSF_{A,h,Ai}$ was determined. Each $FSF_{A,h,Ai}$ was multiplied by the heat transfer coefficient of the corresponding smooth surface. The products were specified as the heat transfer coefficients for the convection boundary condition of the corresponding adapted solid-state simulation model.

According to Section 3.1, a smooth and a finned surface are thermally the same if the heat flows are the same at the same ambient and surface temperatures. The heat flows resulting from the CFD analyses are compared with those of the solid-state simulations to show the thermal similarity. Furthermore, the relative deviation of these heat flows is calculated in each case, with the value from the CFD simulation forming the reference value.

Table 5. The standard deviation of the heat flows results from the different *FSF*s concerning the respective reference heat flows $FSF_{ref,i}$. The smallest deviations are highlighted.

FSF	Overall	T_{fb} (K)					*H* (mm)				*L* (mm)				*b* (mm)		
		303	323	373	423	473	13	25	50	100	125	250	500	8.8	14.7	32.4	56.0
FSF_A	1.40	2.06	1.43	1.07	0.91	0.80	0.44	0.70	1.22	2.13	0.77	1.20	1.78	2.19	0.82	0.44	0.33
$FSF_{A,\eta,EL}$	1.18	1.75	0.91	0.56	0.63	0.77	0.42	0.66	1.13	1.86	0.81	1.07	1.46	1.95	0.81	0.42	0.35
$FSF_{A,\eta,Ai}$	1.17	1.75	0.91	0.55	0.60	0.74	0.42	0.66	1.13	1.85	0.80	1.06	1.45	1.93	0.78	0.40	0.35
$FSF_{A,\eta,Ba}$	1.19	1.77	0.91	0.56	0.63	0.77	0.42	0.66	1.13	1.87	0.81	1.08	1.47	1.97	0.80	0.41	0.35
$FSF_{A,\eta,Ro1}$	1.16	1.77	0.93	0.53	0.56	0.69	0.42	0.66	1.13	1.84	0.78	1.05	1.45	1.93	0.74	0.38	0.33
$FSF_{A,\eta,Ro1\cdot32}$	1.22	1.78	0.92	0.60	0.70	0.85	0.42	0.66	1.15	1.92	0.85	1.12	1.51	2.02	0.87	0.45	0.38
$FSF_{A,\eta,Ol1}$	1.24	1.80	0.96	0.62	0.70	0.85	0.42	0.67	1.16	1.95	0.86	1.13	1.53	2.03	0.89	0.45	0.37
$FSF_{A,\eta,Ol1\cdot32}$	1.32	1.82	0.99	0.73	0.85	1.02	0.42	0.67	1.19	2.05	0.96	1.22	1.61	2.12	1.06	0.54	0.43
$FSF_{A,h,EL}$	0.55	0.51	0.50	0.44	0.39	0.40	0.23	0.31	0.49	0.69	0.63	0.50	0.45	0.68	0.59	0.46	0.26
$FSF_{A,h,Ai}$	0.47	0.38	0.34	0.30	0.31	0.41	0.22	0.30	0.49	0.62	0.51	0.44	0.44	0.63	0.49	0.39	0.23
$FSF_{A,h,Ba}$	0.56	0.58	0.55	0.46	0.38	0.37	0.25	0.33	0.50	0.74	0.65	0.51	0.47	0.72	0.61	0.44	0.25
$FSF_{A,h,Ro1}$	0.49	0.29	0.19	0.24	0.39	0.55	0.21	0.31	0.52	0.61	0.49	0.47	0.51	0.70	0.50	0.34	0.24
$FSF_{A,h,Ro1\cdot32}$	0.96	0.98	1.02	0.98	0.87	0.77	0.30	0.40	0.61	1.17	1.14	0.89	0.71	1.18	1.06	0.71	0.40
$FSF_{A,h,Ol1}$	0.99	1.00	1.02	1.00	0.93	0.86	0.32	0.44	0.70	1.34	1.15	0.89	0.79	1.14	1.11	0.71	0.37
$FSF_{A,h,Ol1\cdot32}$	2.07	1.91	2.08	2.17	2.11	2.01	0.47	0.72	1.22	2.51	2.44	1.90	1.53	2.39	2.43	1.47	0.85
$FSF_{A,\eta,h,EL}$	0.86	0.40	0.44	0.67	0.87	1.06	0.23	0.34	0.66	1.23	0.58	0.78	1.04	1.24	0.91	0.54	0.37
$FSF_{A,\eta,h,Ai}$	0.91	0.38	0.47	0.73	0.95	1.15	0.22	0.34	0.67	1.23	0.65	0.86	1.09	1.32	0.96	0.55	0.39
$FSF_{A,\eta,h,Ba}$	0.85	0.46	0.46	0.65	0.84	1.03	0.25	0.35	0.64	1.20	0.57	0.76	1.03	1.22	0.92	0.55	0.38
$FSF_{A,\eta,h,Ro1}$	1.01	0.46	0.59	0.87	1.09	1.28	0.22	0.34	0.69	1.24	0.81	0.99	1.18	1.45	1.08	0.60	0.44
$FSF_{A,\eta,h,Ro1\cdot32}$	0.83	0.67	0.60	0.63	0.75	0.90	0.29	0.41	0.70	1.35	0.60	0.61	0.93	1.17	0.89	0.57	0.35
$FSF_{A,\eta,h,Ol1}$	0.89	0.76	0.69	0.73	0.84	0.98	0.31	0.44	0.75	1.43	0.60	0.69	1.03	1.24	0.88	0.58	0.36
$FSF_{A,\eta,h,Ol1\cdot32}$	1.28	1.35	1.27	1.19	1.15	1.17	0.46	0.68	1.12	2.08	1.31	0.83	1.00	1.64	1.36	0.87	0.49

Table 6 lists all dimensions, isothermal boundary conditions, and the simulations' results.

Table 6. Dimensions, boundary conditions, output and relative deviation of the finned arrays.

Parameter	**Unit**	**Examples from Literature**								
Source	**-**	**[25]**			**[26]**			**[27]**		
s	mm	5.00			25.00			4.00		
W	mm	180.00			150.00			250.00		
B	mm	3.00			2.00			3.00		
H	mm	25.00			50.00			15.00		
L	mm	340.00			200.00			100.00		
b	mm	14.70			16.50			16.00		
n	-	11.00			9.00			14.00		
k_f	W/m K	130.00			200.00			200.00		
T_∞	K	293.00			301.30			293.00		
T_{fb}	K	314.5	339.0	360.0	314.3	333.8	351.8	323.0	338.0	353.0
h_{vp}	W/m^2 K	4.37	5.34	5.86	4.01	5.12	5.73	5.68	6.27	6.70
$FSF_{A,h,Ai}$	-	3.66	3.64	3.62	7.01	6.94	6.89	2.85	2.83	2.82
Q_{CFD}	W	18.48	50.20	82.26	10.99	35.89	63.54	11.06	18.76	27.50
$Q_{FEA+FSF}$	W	21.03	54.74	87.01	10.93	34.50	59.43	12.11	19.96	27.38
Dev.	%	13.77	9.04	5.77	−0.57	−3.88	−6.47	9.48	6.39	−0.45

4. Discussion and Conclusions

The overarching goal of the authors' research is to accelerate heat transfer simulations of finned arrays. For this purpose, the authors have defined the *FSF* and developed a process whose output is the most accurate analytical *FSF* calculation path for a given case. The performance of the approach was demonstrated using the example of a vertical finned array under natural convection with an isothermal temperature at the fin base. Based on

this case study and the results presented in Tables 4 and 5, the following conclusions can be drawn:

1. *FSF*s were determined based solely on geometric ratios, and the heat conduction showed the largest deviations both overall and concerning low-level parameters. Thus, these calculation paths were unsuitable.
2. The same applies to the calculation paths, which consider all three components. Looking at all, the results $FSF_{A,\eta,h,EL}$ were the exception, as this calculation path was among the five most accurate ones.
3. The paths considering the geometric and heat transfer components gave the best results. Four of the five most accurate calculation paths were among these concerning the overall mean deviation and the overall standard deviation. The $FSF_{A,h,Ro1}$ path had the best results for low fin base temperatures. There was no single calculation path for higher temperatures and different fin heights that turned out to be particularly accurate. The performance of the $FSF_{A,h,El}$, $FSF_{A,h,Ai}$, $FSF_{A,h,Ba}$ and $FSF_{A,h,Ro1}$ paths were very similar for these parameters. For longer fin lengths and almost all examined fin spacing, the $FSF_{A,h,Ai}$ path was the best one.
4. The $FSF_{A,h,Ai}$ path gave the best results with an 8% overall mean deviation and an overall standard deviation of 0.5. For this reason, this calculation path is recommended for the analytical determination of the *FSF* for vertical rectangular finned arrays considering natural convection with air as surrounding fluid and an isothermal boundary condition.

In Section 3.3.4. the $FSF_{A,h,Ai}$ path was verified using three different fin arrays at three different temperatures. The deviation between the results of the CFD simulations and the solid-state simulations (FEA) using the $FSF_{A,h,Ai}$ were between −6.47% and 13.77%. The average relative deviation according to the amount of overall simulations was 6.2%. In light of these results, the approach presented in this work is suitable for accelerating thermal simulations and achieves sufficiently accurate results simultaneously.

As an alternative to the methods presented or used in [9–11] to substitute cooling fins, our approach offers an analytical solution. Provided that the corresponding formulas and correlations are available or that existing ones can be transferred, thermal simulations of any fin geometries and orientations can be simplified under various boundary conditions. The technical benefit of the approach becomes evident when correspondingly large and complex components are considered, such as large transformers or dry storage casks for spent fuel assemblies.

The authors' future research focuses on defining different analytical calculation paths, e.g., for constant heat flow boundary conditions instead of an isothermal one or other fin shapes and orientations. In addition to natural convection, radiation-related heat transfer should also be considered to depict real problems with *FSF* more precisely.

Author Contributions: Conceptualization, methodology, validation, investigation, writing—original draft preparation, M.R.; writing—review and editing, supervision, S.T. and F.R. All authors have read and agreed to the published version of the manuscript.

Funding: Funded by the Deutsche Forschungsgemeinschaft (DFG, German Research Foundation)—491183248. Funded by the Open Access Publishing Fund of the University of Bayreuth.

Institutional Review Board Statement: Not applicable.

Informed Consent Statement: Not applicable.

Data Availability Statement: Not applicable.

Conflicts of Interest: The authors declare no conflict of interest. The funders had no role in the design of the study; in the collection, analyses, or interpretation of data; in the writing of the manuscript, or in the decision to publish the results.

Nomenclature

A_0	area smooth surface
A_{fa}	area finned array
A_{fb}	area fin base
A_f	area of all fins
$A_{f,cs}$	cross-sectional area of one fine
$A_{f,s}$	area of one fin
B	fin width
b	fin spacing
Bi	Biot number
c_{Ro}	Rohsenow parameter
C_{Ro}	Rohsenow parameter
CFD	Computational fluid dynamics
c_p	specific heat capacity
FEM	Finite-Element-Method
FSF	fin substitution factor
g	acceleration of gravity
H	fin hight
h	heat transfer coefficient
h_0	heat transfer coefficient smooth surface
h_f	heat transfer coefficient finned array
k_{fluid}	conductivity fluid
k_f	conductivity fins
L	fin length
L_{spe}	specific length
n	number of fins
Nu	Nusselt number
P_f	perimeter of one fin
Pr	Prandtl number
Q_0	Heat flux smooth surface
Q_{CFD}	Heat flux flow simulation
Q_f	Heat flux finned array
$Q_{FEM+FSF}$	Heat flux solid-state simulation
Ra	Rayleigh number
s	base plate thickness
T_∞	ambient temperature
T_S	surface temperature
T_{fb}	fin base temperature
W	base plate width
$y+$	dimensionless wall distance
α	thermal diffusivity
β	thermal expansion coefficient
η_f	fin efficiency
μ	fin parameter
ν	kinematic viscosity
ρ	density

References

1. Senapati, J.R.; Dash, S.K.; Roy, S. Numerical investigation of natural convection heat transfer from vertical cylinder with annular fins. *Int. J. Therm. Sci.* **2017**, *111*, 146–159. [CrossRef]
2. Senapati, J.R.; Dash, S.K.; Roy, S. Numerical investigation of natural convection heat transfer over annular finned horizontal cylinder. *Int. J. Heat Mass Transf.* **2016**, *96*, 330–345. [CrossRef]
3. Wong, S.-C.; Lee, W.-Y. Numerical study on the natural convection from horizontal finned tubes with small and large fin temperature variations. *Int. J. Therm. Sci.* **2019**, *138*, 116–123. [CrossRef]
4. Mehrtash, M.; Tari, I. A correlation for natural convection heat transfer from inclined plate-finned heat sinks. *Appl. Therm. Eng.* **2013**, *51*, 1067–1075. [CrossRef]

5. Tari, I.; Mehrtash, M. Natural convection heat transfer from inclined plate-fin heat sinks. *Int. J. Heat Mass Transf.* **2013**, *56*, 574–593. [CrossRef]
6. Shen, Q.; Sun, D.; Xu, Y.; Jin, T.; Zhao, X. Orientation effects on natural convection heat dissipation of rectangular fin heat sinks mounted on LEDs. *Int. J. Heat Mass Transf.* **2014**, *75*, 462–469. [CrossRef]
7. Incropera, F.P.; Dewitt, D.P.; Bergman, T.L.; Livine, A.S. *Introduction to Heat Transfer*, 5th ed.; John Wily & Son: New York, NY, USA, 2007; pp. 348–372.
8. Clapp, M. *A Designer's Guide to CFD*, 1st ed.; NAFEMS: Hamilton, ON, Canada, 2019.
9. Xu, Y.; Yang, J.; Xu, C.; Wang, W.; Ma, Z. Thermal analysis on NAC-STC spent fuel transport cask under different transport conditions. *Nucl. Eng. Des.* **2013**, *265*, 682–690. [CrossRef]
10. Leber, A.; Graf, W.; Hüggenberg, R. Validation of CFD-methods to predict heat transfer and temperatures during the transport and storage of casks under a cover. In Proceedings of the 14th International Symposium on the Packaging and Paper Transportation of Radioactive Materials (PATRAM), Berlin, Germany, 20–24 September 2004.
11. Stratmann, W.; Hages, P. Analysis of removal of residual decay heat from interim storage facilities by means of the CFD program FLUENT. In Proceedings of the 14th International Symposium on the Packaging and Paper Transportation of Radioactive Materials (PATRAM), Berlin, Germany, 20–24 September 2004.
12. ANSYS Inc. *ANSYS FLUENT 2020 R2: ANSYS FLUENT User´s Guide*; ANSYS Inc.: Canonsburg, PA, USA, 2020.
13. *VDI Heat Atlas*, 2nd ed.; Springer: Berlin/Heidelberg, Germany, 2010. [CrossRef]
14. Karwa, R. *Heat and Mass Transfer*, 2nd ed.; Springer Nature: Singapore, 2020. [CrossRef]
15. Churchill, S.W.; Chu, H.H.S. Correlating equations for laminar and turbulent free convection from a vertical plate. *Int. J. Heat Mass Transf.* **1975**, *18*, 1323–1329. [CrossRef]
16. Marek, R.; Nitsche, K. *Praxis der Wärmeübertragung*, 5th ed.; Carl Hanser Verlag: München, Germany, 2019; pp. 192–194.
17. Kraus, A.D.; Aziz, A.; Welty, J. *Extended Surface Heat Transfer*, 1st ed.; John Wily & Son: New York, NY, USA, 2001; pp. 190–207.
18. Elenbaas, W. Heat dissipation of parallel plates by free convection. *Physica* **1942**, *9*, 1–28. [CrossRef]
19. Auhara, T. Heat Transfer due to Natural Convection from Parallel Vertical Plates. *Trans. Jpn. Soc. Mech. Engr.* **1963**, *29*, 903–909. [CrossRef]
20. Bar-Cohen, A.; Rohsenow, W.M. Thermally Optimum Spacing of Vertical, Natural Convection Cooled, Parallel Plates. *J. Heat Transf.* **1984**, *106*, 116–123. [CrossRef]
21. Rohsenow, W.M.; Hartnett, J.P.; Cho, Y.I. *Handbook of Heat Transfer*, 3rd ed.; McGraw-Hill: New York, NY, USA, 1998; pp. 4.1–4.40.
22. Olsson, C.-O. Prediction of Nusselt Number and Flow Rate of Buoyancy Driven Flow Between Vertical Parallel Plates. *J. Heat Transf.* **2004**, *126*, 97–104. [CrossRef]
23. Wu, T.; Lei, C. On numerical modelling of conjugate turbulent natural convection and radiation in a differentially heated cavity. *Int. J. Heat Mass Transf.* **2015**, *91*, 454–466. [CrossRef]
24. Jeong, H.M.; Lee, Y.H.; Ji, M.K.; Bae, K.Y.; Chung, H.S. Natural convection heat transfer estimation from a longitudinally finned vertical pipe using CFD. *J. Mech. Sci. Technol.* **2009**, *23*, 1517–1527. [CrossRef]
25. Yazicioğlu, B.; Yüncü, H. Optimum fin spacing of rectangular fins on a vertical base in free convection heat transfer. *Heat Mass Transf.* **2006**, *44*, 11–21. [CrossRef]
26. Sathe, A.; Sanap, S.; Dingare, S.; Sane, N. Thermal Analysis of Vertical Plate Fin Heat Sink. *E3S Web Conf.* **2020**, *170*, 01022. [CrossRef]
27. Güvenç, A.; Yüncü, H. An experimental investigation on performance of fins on a horizontal base free convective heat transfer. *Heat Mass Transf.* **2001**, *37*, 409–416. [CrossRef]